

# Quasi-Elastic Neutron Scattering Studies on Dynamics of Water Confined in Nanoporous Copper Rubeanate Hydrates

Takeshi Yamada,<sup>†,‡</sup> Ryo Yonamine,<sup>†</sup> Teppei Yamada,<sup>‡,§</sup> Hiroshi Kitagawa,<sup>‡,§</sup> Madhusudan Tyagi,<sup>§,||</sup> Michihiro Nagao,<sup>§,⊥</sup> and Osamu Yamamuro<sup>\*,†,‡</sup>

<sup>†</sup>Neutron Science Laboratory, Institute for Solid State Physics, The University of Tokyo, 5-1-5 Kashiwanoha, Kashiwa, Chiba 277-8581, Japan

<sup>‡</sup>Graduate School of Science, Kyoto University, Kitashirakawa Oiwake-cho, Sakyo-ku, Kyoto 606-8502, Japan

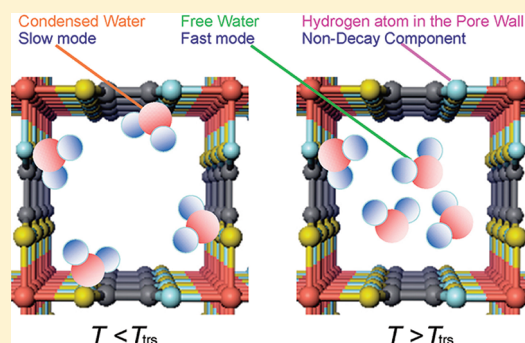
<sup>§</sup>NIST Center for Neutron Research, National Institute of Standards and Technology, 100 Bureau Drive, Gaithersburg, Maryland 20899-6102, United States

<sup>||</sup>Department of Materials Science and Engineering, University of Maryland, College Park, Maryland, 20742-2115, United States

<sup>⊥</sup>Center for Exploration of Energy and Matter, Indiana University, Bloomington, Indiana 47408-1398, United States

<sup>\*</sup>JST-CREST, 5 Sanban-cho, Chiyoda-ku, Tokyo 102-0075, Japan

**ABSTRACT:** We have investigated the mechanism of the first order transition and proton conductivity in copper rubeanate hydrates from microscopic and dynamical points of view. Three different types of neutron spectrometer—time-of-flight, backscattering, and neutron spin echo—were used to cover a wide dynamic range (1 ps to 100 ns). We found that the water molecules adsorbed in the pore are divided into “free water” having diffusion coefficients similar to those of bulk water at room temperature and “condensed water” which is about 10 times slower than bulk water owing to the interaction with the pore wall. The hydrogen atoms in the pore wall exhibited no relaxation within the measured time scales. The free water has, in the framework of the jump-diffusion model, smaller activation energy, longer residence time, and longer jump distance than bulk water. The neutron spin echo measurement revealed that the first order transition is a kind of liquid–liquid transition at which the free water is condensed on the pore surface in the low temperature phase. On cooling the condensed water, the relaxation time starts to deviate from the VFT equation around 200 K as previously observed in the water confined in nanoporous silicates. The free water plays an important role as the proton carrier but the proton conductivity is mainly governed by the number of protons provided into the adsorbed water from the pore wall.



## 1. INTRODUCTION

In our life, water is one of the most essential materials. Meanwhile, the physical properties as a liquid, for example the maximum density at 4 °C, are quite different from ordinary liquids.<sup>1</sup> One of the proposed models for explaining this anomaly is based on the existence of the transition between low-density water (LDW) and high-density water (HDW) in a supercooled temperature region below the homogeneous nucleation temperature ( $T_h$ ).<sup>2–5</sup> In the experimental studies on the LDW–HDW transition, water confined in nanosized spaces, in materials such as mesoporous silicate, carbon nanotubes, or zeolites, is widely used to suppress crystallization. Of course, other phenomena owing to the size and surface effects occur in these systems, e.g. change of fusion temperature and slowing of diffusion of the confined water.

Cold neutrons have angstrom wavelengths, and given the large incoherent scattering cross-section of hydrogen atoms, quasi-elastic neutron scattering (QENS) is an appropriate method to investigate the dynamics of water at a nanoscopic level. It has been widely used in the studies on the dynamics of bulk water<sup>6</sup> and confined water.<sup>7–11</sup> For example, Liu et al. reported that the

translational relaxation of water confined in mesoporous silicate MCM-41 exhibits a transition from non-Arrhenius type (HDW) to Arrhenius type (LDW) at 225 K on cooling.<sup>8</sup> This behavior is sometimes called the “Fragile–Strong” transition as used in glass forming liquids. Yoshida et al. also reported a similar transition at 230 K using the neutron spin echo (NSE) technique.<sup>9</sup> Similar phenomena were observed also in water confined in double-wall carbon nanotubes at 190 K<sup>10</sup> and water on CeO<sub>2</sub> surfaces at 215 K<sup>11</sup> and discussed in accordance with the LDW–HDW transition. Meanwhile the confinement effects on the dynamics of water have also been investigated by QENS. Kamitakahara and Wada reported that the water confined in zeolites shows 2 orders of magnitude slower dynamics than that of bulk water and that this is governed by ionic charges in the zeolite.<sup>12</sup> Malikova et al. demonstrated that the intercalated water between clay layers exhibits two-dimensional diffusion.<sup>13</sup>

Received: March 30, 2011

Revised: October 13, 2011

Published: October 14, 2011

Copper rubeanate ( $\text{H}_2\text{C}_2\text{N}_2\text{S}_2\text{Cu}$ ;  $\text{H}_2\text{dtoaCu}$ ) used in this study is a porous coordinate metal complex where rubeanic acids coordinate to copper ions. The size of the nearly rectangular pore is about 0.7 nm.  $\text{H}_2\text{dtoaCu}$  adsorbs water in the pore as a function of relative humidity (RH) and gives high proton conductivity.<sup>14</sup> The maximum hydration number at RH = 100% is about 4, which is reasonable considering the size of the pore and water molecule. The proton conductivity at this condition reaches  $10^{-2} \text{ Scm}^{-1}$  which is the same as that of Nafion membrane which is known as the best commercial proton conductor. We have investigated the structures and heat capacities ( $C_p$ ) of the copper rubeanate hydrates ( $\text{H}_2\text{dtoaCu} \cdot n\text{H}_2\text{O}$ ) having different hydration number by neutron powder diffraction and heat capacity measurements.<sup>15</sup> The  $C_p$  measurement of the sample with  $n = 3.7$  revealed that a glass transition and a first order transition originating from the adsorbed water appear at 150 K ( $T_g$ ) and 260 K ( $T_{\text{ts}}$ ), respectively. The first-order nature was revealed by long endothermic drifts during the equilibration periods in adiabatic calorimetry. This transition exhibits a long  $C_p$  tail in the low temperature side. The transition entropy of the first order transition is similar to the melting entropy of bulk water, suggesting that the adsorbed water molecules are disordered as much as those in bulk water above 260 K. Neutron powder diffraction data showed that the structures of  $\text{H}_2\text{dtoaCu} \cdot n\text{H}_2\text{O}$  are amorphous in the whole measured temperature range over  $T_{\text{ts}}$ . From these results, we suggested that the 260 K transition is associated with the ordering of water molecules in the pores.<sup>15</sup>

In this paper, we report several results of the QENS experiments of  $\text{H}_2\text{dtoaCu} \cdot n\text{H}_2\text{O}$  and discuss the mechanism of the transition from microscopic and dynamical points of view. The mechanism of proton conductivity, which is another interest in this material, is also discussed.

## 2. EXPERIMENTAL SECTION

**2.1. Samples.**  $\text{H}_2\text{dtoaCu}$  was prepared by simple mixing of a dithiooxamide aqueous solution and a copper sulfate solution, as described elsewhere.<sup>14</sup> The copper rubeanate hydrates were prepared by putting the samples in a glovebag with RH = 100%. The extent of hydration was adjusted by the exposure time, e.g., several hours for less hydrated samples and a few days for the full hydrated sample. The hydration number was precisely determined by weighing the hydrated and dry samples. The completely dry sample was prepared under vacuum at 50 °C for 24 h. The samples prepared for this study were  $\text{H}_2\text{dtoaCu} \cdot n\text{H}_2\text{O}$  ( $n = 0, 1.3, 2.1, 3.7$ ). Only  $\text{H}_2\text{dtoaCu} \cdot 3.7\text{H}_2\text{O}$  is used in the NSE and HFBS experiments.

**2.2. Instruments and Measurements.** The dynamics of water in the pores of copper rubeanate was investigated using the following three experiments employing different neutron spectrometers having different energy resolutions. The relaxation time region covered by these experiments is from 1 ps to 100 ns (5 order of magnitude). This is almost the widest limit accessible in the current neutron scattering techniques.

**2.2.1. Time of Flight Method.** The QENS and fixed window scan of  $\text{H}_2\text{dtoaCu} \cdot n\text{H}_2\text{O}$  were performed using a time-of-flight spectrometer AGNES<sup>16</sup> owned by the Institute for Solid State Physics, The University of Tokyo. This instrument is installed at the cold neutron guide (C3-1) of the research reactor, JRR-3 of Japan Atomic Energy Agency (JAEA). Neutrons with a wavelength of 0.422 nm (for standard mode) or 0.550 nm (for high resolution mode) are extracted with an array of five PG(002) monochromators and pulsed with a double Fermi chopper. The pulsed neutrons are scattered by a sample and detected with  $^3\text{He}$  tube detectors arranged in a wide detector bank covering the scattering angles of 10–130°. The energy

resolution, energy range, and scattering vector,  $Q$  range at the standard mode, which was used in this experiment, are  $120 \mu\text{eV}$ ,  $-4 \text{ meV} < \Delta E < 20 \text{ meV}$ , and  $2 \text{ nm}^{-1} < Q < 27 \text{ nm}^{-1}$ , respectively. The powder samples were wrapped with aluminum foils and loaded into the concentric double cylinder aluminum cell (50 mm in height, 14.0 mm in inner diameter of the outer cylinder, 12.0 mm in outer diameter of the inner cylinder) in a globe bag with helium atmosphere and 100% RH. Considering the samples were in powder form, the effective sample thickness was about 0.5 mm and the transmission of neutrons was about 0.9. This sample can was also used in the backscattering spectrometer described next. In the fixed window scans, the intensity was recorded roughly at every 10 K from 100 to 340 K. It takes 1 h for each point. The quasi-elastic scattering data were recorded at 150 (for resolution), 268, 284, 300, 320, and 340 K with a counting time of 8 h. Bulk water was also measured for comparison.

**2.2.2. Backscattering.** Neutron backscattering was performed using the high-flux backscattering spectrometer<sup>17</sup> (HFBS) at the NG2 of the guide hall at the NIST Center for Neutron Research (NCNR) of National Institute of Standards and Technology (NIST, USA). The incident neutron wavelength at the HFBS is varied via Doppler shifting about a nominal value of 0.6271 nm ( $E_0 = 2.08 \text{ meV}$ ). After scattering from the sample, only neutrons having a fixed final energy of 2.08 meV are measured by the detectors as ensured by Bragg reflection from analyzer crystals Si(111). The instrument was operated with dynamic ranges of  $\pm 11$  and  $\pm 17 \mu\text{eV}$ . With these dynamic ranges, full width of the sample-dependent instrument resolution function at half-maximum was  $0.85 \mu\text{eV}$ , as measured with the vanadium standard. The data collected at 15 detectors  $2.5 \text{ nm}^{-1} < Q < 17 \text{ nm}^{-1}$  (at the elastic channel) were used in the data analysis. The DAVE software package was used to reduce the HFBS data.<sup>18</sup> The same sample as used in the AGNES experiment was used in the HFBS experiment. The fixed window scan was performed from 4 to 340 K with  $1 \text{ K min}^{-1}$ . The QENS spectra were measured at 4 (for resolution), 220, 242, 262, 282, 300, and 322 K. The counting time of each QENS measurement was 8 h.

**2.2.3. Neutron Spin Echo.** Neutron spin echo experiments were performed using the NG5-NSE spectrometer<sup>19</sup> at the NCNR. The spectrometer is installed at the NG5 of the guide hall at the NCNR. The beamline includes a neutron velocity selector to choose a neutron wavelength, a transmission polarizer and a reflection analyzer for the capability of neutron polarization analyses, and two-dimensional area detector. The wavelength of used neutrons was 0.6 nm with a wavelength resolution of about 20%. The temperature was controlled with a closed cycle refrigerator. The DAVE software package was used to reduce the NSE data from the echo signal to the intermediate scattering function.<sup>18</sup>

Coherent scattering is usually observed in NSE measurements in order to investigate a relaxation of a specific correlation defined by  $Q$ . In the present experiment, however, incoherent scattering was measured from the hydrogenated sample for comparison with the results of other spectrometers. The scattering vector was chosen at  $Q = 7 \text{ nm}^{-1}$  to avoid scattering from the cell and coherent peak. The data were taken at 180, 200, 220, 240, 260, 280, 300, and 340 K and at Fourier times between 0.007 and 15 ns. The resolution data were taken at 50 K. The total counting time at each temperature was 21 h. The powder sample of  $\text{H}_2\text{dtoaCu} \cdot 3.7\text{H}_2\text{O}$  was loaded into a concentric double cylinder aluminum cell (50 mm in height, 30.0 mm in inner diameter of the outer cylinder, 28.0 mm in outer diameter of the inner cylinder) in the globebag following the procedure used for AGNES.

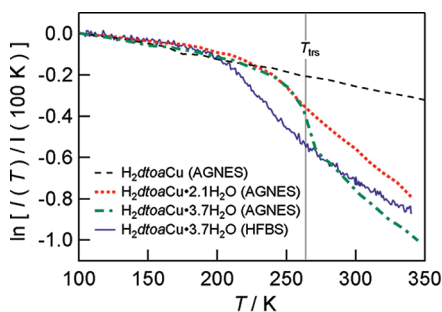


**Figure 1.** Normalized elastic scattering intensities of  $\text{H}_2\text{dtoaCu}$  (dashed line),  $\text{H}_2\text{dtoaCu}\cdot 2.1\text{H}_2\text{O}$  (dotted line), and  $\text{H}_2\text{dtoaCu}\cdot 3.7\text{H}_2\text{O}$  (dashed dotted line) as a function of temperature measured by AGNES. The solid curve is  $\text{H}_2\text{dtoaCu}\cdot 3.7\text{H}_2\text{O}$  measured by HFBS. The average  $Q$  values of the AGNES and HFBS measurements are 14 and  $10\text{ nm}^{-1}$ , respectively.

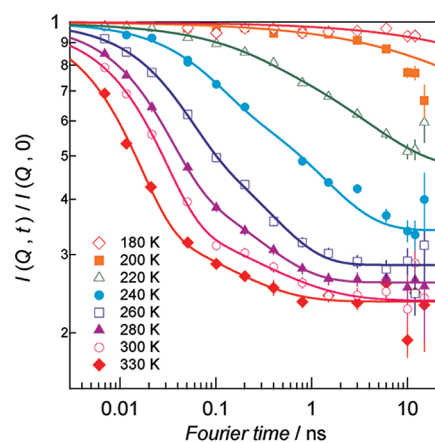


**Figure 2.** Incoherent intermediate scattering functions of  $\text{H}_2\text{dtoaCu}\cdot 3.7\text{H}_2\text{O}$  obtained by NSE at  $Q = 7\text{ nm}^{-1}$ . Solid curves are the results of the fittings to eq 1. Error bars represent a  $\pm 1$  standard deviation through out the paper.

### 3. RESULTS AND DISCUSSION

**3.1. Fixed Window Scan.** Figure 1 shows normalized elastic scattering intensities of  $\text{H}_2\text{dtoaCu}\cdot n\text{H}_2\text{O}$  obtained by AGNES and HFBS. This plot is linear for a harmonic oscillator and so the deviation from the straight line indicates an anharmonic vibration and/or relaxation in the samples. The data of  $\text{H}_2\text{dtoaCu}$ , a dry sample, exhibited a nearly linear temperature-dependence in the whole temperature range. In the hydrated samples ( $n = 2.1$  and  $3.7$ ), however, a deviation from the linear relationship appeared above 240 K in AGNES and above 200 K in HFBS data. It is reasonable that HFBS has a lower deviation temperature than AGNES even for a single relaxation mode since the former has 100 times better energy resolution (slower time scale) than the latter. Taking the consistency with the results described below into consideration, however, we attribute the difference between HFBS and AGNES data to two kinds of relaxation modes having different relaxation times in the adsorbed water. We call these modes “fast mode” and “slow mode” in this paper. In the AGNES data of  $\text{H}_2\text{dtoaCu}\cdot 3.7\text{H}_2\text{O}$ , a jump of intensity appeared at 260 K, which is the first order transition temperature observed in the heat capacity measurement,<sup>15</sup> whereas just a small kink appeared around 260 K in the HFBS data. These data indicate that the fast mode mainly relates to the first order transition.

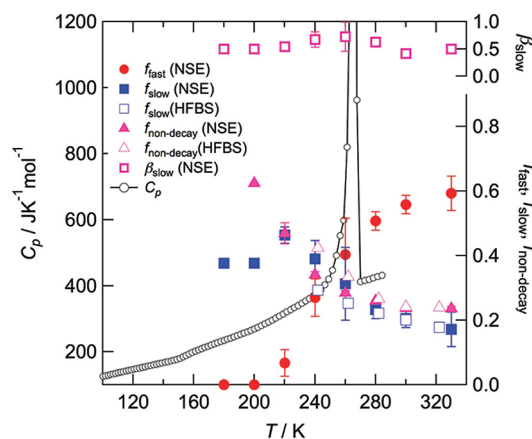


**Figure 3.** Temperature dependence of the fraction of each relaxation component and  $\beta_{\text{slow}}$  of slow-mode in  $\text{H}_2\text{dtoaCu}\cdot 3.7\text{H}_2\text{O}$ . The heat capacities<sup>15</sup> are also plotted for comparison.

**3.2. Neutron Spin Echo.** Figure 2 shows incoherent intermediate scattering function of  $\text{H}_2\text{dtoaCu}\cdot 3.7\text{H}_2\text{O}$  obtained by NSE. A single relaxation was observed below 240 K which is near  $T_{\text{trs}}$  whereas two relaxations were observed above 240 K. Additionally a nondecay component was observed in the whole temperature range. These two relaxations correspond to the two relaxations observed by the fixed window scan (fast mode and slow mode). These data were fitted to the following equations:

$$\frac{I(Q, t)}{I(Q, 0)} = f_{\text{fast}} \exp\left(-\frac{t}{\tau_{\text{fast}}}\right) + f_{\text{slow}} \exp\left(-\left(\frac{t}{\tau_{\text{slow}}}\right)^{\beta_{\text{slow}}}\right) + f_{\text{nondecay}} \quad (1)$$

$$f_{\text{fast}} + f_{\text{slow}} + f_{\text{nondecay}} = 1 \quad (2)$$

where the first term of eq 1 is an exponential function corresponding to the fast mode and the second term is a stretched exponential function corresponding to the slow mode and the third term is a constant corresponding to the nondecay component. The parameter  $f$  is a fraction of each component and  $\tau$  is a relaxation time and  $\beta$  is a nonexponential parameter ( $\beta = 1$  for the exponential decay). Though the statistical error is large in the long Fourier time region, all of the data were fitted well to eq 1 in the whole measured temperature range.

Figure 3 shows the temperature dependence of the fraction of each relaxation component. The heat capacities of  $\text{H}_2\text{dtoaCu}\cdot 3.7\text{H}_2\text{O}$  are also plotted for comparison.<sup>15</sup> On cooling the sample, the fast mode disappeared around the first order transition temperature. The temperature where  $f_{\text{fast}}$  changes most steeply agrees with the  $C_p$  peak temperature (260 K) and  $f_{\text{fast}}$  vanishes at the  $C_p$  rising temperature (200 K). The slow mode and the nondecay component increased gradually. The  $\beta_{\text{slow}}$  was about 0.5 in the whole temperature region. Both on the present data and our previous data,<sup>15</sup> we propose that the first order transition is due to the condensation of the free water on the surface of the pores. The fast mode is associated with the free water and the slow mode with the condensed water. It is plausible that the motion of the condensed water having strong correlation with the surface is described as a stretched exponential function with  $\beta = 0.5$ . The orientation of the condensed water is considered to be gradually ordered on cooling and frozen-in at

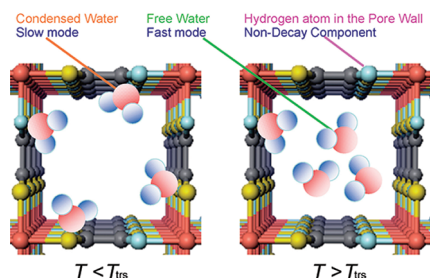


**Figure 4.** Illustration of the water molecules in the pore of copper rubeanate below (left) and above (right) the first order transition temperature.

the glass transition temperature (150 K). This gradual ordering is consistent with the excess entropy data;<sup>15</sup> about 50% of excess entropy is gained below the transition temperature (260 K). The transition mechanism is schematically shown in Figure 4. In this illustration, four water molecules are put in the pore and arranged in arbitrary manners in both phases. Figure 4 shows that some of the free-water molecules are condensed even at  $T > T_{\text{trs}}$ , and further condensation occurs through the transition on cooling. It should be noted that the condensation is completed at a temperature much lower than  $T_{\text{trs}}$  (around 200 K) in the actual transition process.

The temperature dependence of the nondecay component is somewhat strange; it increases with decreasing temperature even below  $T_{\text{trs}}$ . We guess that the nondecay component is attributed to hydrogen atoms in the pore walls and in immobile condensed water. The latter component increases with decreasing temperature. It is plausible that some of the water molecules are rather strongly bound by the NH group of rubeanic acid below  $T_{\text{trs}}$  and do not move in the time scale of NSE. The  $f_{\text{nondecay}}$  at 330 K was 0.24, corresponding to the fraction of hydrogen atoms in the pore wall calculated from the molecular formulas;  $2/(2 + 3.7 \times 2) = 0.21$ . The numerator of this equation is the number of H atoms in copper rubeanate ( $\text{H}_2\text{C}_2\text{N}_2\text{S}_2\text{Cu}$ ), and the denominator is the total number of H atoms in the copper rubeanate hydrate ( $\text{H}_2\text{C}_2\text{N}_2\text{S}_2\text{Cu} \cdot 3.7\text{H}_2\text{O}$ ).

Previously several studies are reported for transitions on substrate surfaces or in pores. For example, deuterated ethylene on graphite surface shows a variety of transitions depending on the coverage, i.e., the transition between solid-film and liquid-film, between the liquid-film and the two-dimensional gas, and the transition accompanying the thickness change of the liquid-films (layering transition).<sup>20</sup> Similar transitions were reported for argon adsorbed on graphite surface.<sup>21</sup> Molecular dynamics simulations for confined water in a hydrophilic surface pore show that the layering transition occurs and the water molecules condensate on the surface of the pores depending on the interaction strength between the water molecules and the pore surface.<sup>22</sup> Our transition of the  $\text{H}_2\text{dtoaCu} \cdot n\text{H}_2\text{O}$  might be similar to these layering transitions.

**3.3. Quasi-Elastic Scattering at AGNES.** Quasi-elastic scattering was observed at several temperatures above 240 K. The data were fitted to the following equations:

$$S(Q, \omega) = \left\{ \delta(\omega) + \exp\left(-\frac{Q\langle u \rangle^2}{3}\right) L_{\text{Trans}}(Q, \omega) \otimes L_{\text{Rot}}(Q, \omega) \right\} \otimes R(Q, \omega) + \text{BG} \quad (3)$$

$$L_{\text{Trans}}(Q, \omega) = \frac{1}{\pi} \frac{\Gamma_s(Q)}{\pi[\omega^2 + \Gamma_s(Q)^2]} \quad (4)$$

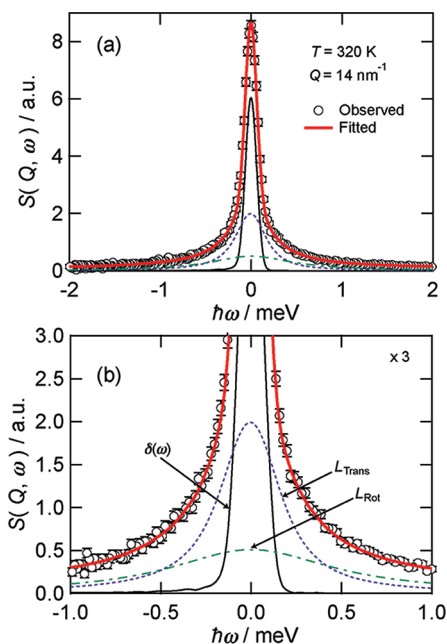


**Figure 5.** QENS profile of  $\text{H}_2\text{dtoaCu} \cdot 3.7\text{H}_2\text{O}$  obtained by AGNES at  $Q = 14 \text{ nm}^{-1}$  and  $T = 320 \text{ K}$ . The bold solid curve is the result of fitting to eq 3. The thin solid, dotted, and dashed curves are  $\delta(\omega)$ ,  $L_{\text{Trans}}$ , and  $L_{\text{Rot}}$  in eq 3, respectively. The scales of vertical and horizontal axes of panel b are enlarged by 3 and 2 times those of panel a, respectively.

$$L_{\text{Rot}}(Q, \omega) = j_0^2(Qa)\delta(\omega) + \frac{1}{\pi} \sum_{l=1}^{\infty} (2l+1)j_l^2(Qa) \frac{l(l+1)D_{\text{rot}}}{\omega^2 + [l(l+1)D_{\text{rot}}]^2} \quad (5)$$

$$\Gamma_s(Q) = \frac{DQ^2}{1 + DQ^2\tau_0} \quad (6)$$

$$\langle l \rangle = (6D\tau_0)^{1/2} \quad (7)$$

$$\tau_{\text{rot}} = \frac{1}{6D_{\text{rot}}} \quad (8)$$

$\delta(\omega)$  in eq 3 is attributed to the scattering from the water molecules with slow mode and the hydrogen atoms in the pore wall ( $\text{H}_2\text{dtoaCu}$ ), whereas the Lorentzian function in eq 3 is from the fast mode of the water molecules. For the fast mode, both translation  $L_{\text{Trans}}(Q, \omega)$  and rotation  $L_{\text{Rot}}(Q, \omega)$  of the water molecules<sup>6</sup> are considered, and they are given in eqs 4 and 5, respectively. The terms  $R(Q, \omega)$  and BG in eq 3 are the resolution function and constant background, respectively. Assuming the jump-diffusion model for the translation, the half-width at half-maximum of  $L_{\text{Trans}}(Q, \omega)$  is given by eq 6 where  $D$  is a self-diffusion coefficient and  $\tau_0$  is a mean residence time. A mean jump distance  $\langle l \rangle$  is given by eq 7. The rotational relaxation time  $\tau_{\text{rot}}$  relates to the diffusion constant  $D_{\text{rot}}$  by eq 8.

All of the data having different  $Q$  values were fitted simultaneously under the constraints satisfying eqs 4–6 (global fitting). Good fittings were obtained in the whole  $Q$  range as shown in Figure 5. Figure 6 shows Arrhenius plots of the self-diffusion coefficient  $D$ ,  $\tau_0$ ,  $\langle l \rangle$ , and  $\tau_{\text{rot}}$  obtained by the fitting. Activation energies are obtained from the slope of the plots of  $D$  and  $\tau$ 's and are listed in Table 1. All of the activation energies of  $\text{H}_2\text{dtoaCu} \cdot n\text{H}_2\text{O}$

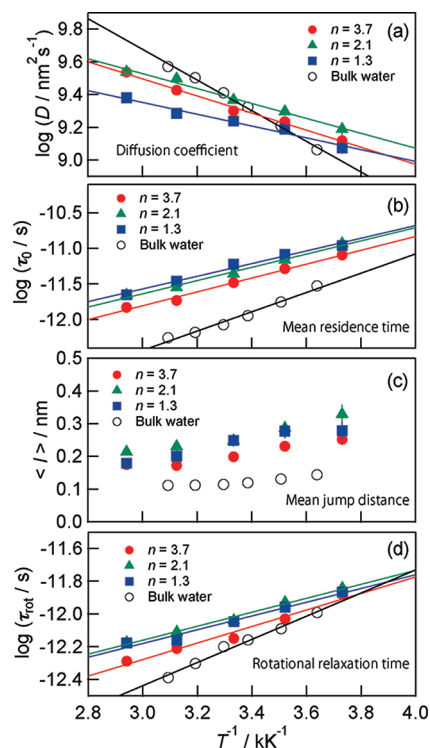


**Figure 6.** Arrhenius plots for (a) diffusion coefficients, (b) mean residence times, (c) mean jump distances, and (d) rotational relaxation times of  $\text{H}_2\text{dtoaCu} \cdot 3.7\text{H}_2\text{O}$  and bulk water.

**Table 1.** Activation Energies Obtained from the Temperature Dependence of Diffusion Coefficients ( $D$ ), Mean Residence Times ( $\tau_0$ ), and Rotational Relaxation Times ( $\tau_{\text{rot}}$ ) for  $\text{H}_2\text{dtoaCu} \cdot n\text{H}_2\text{O}$  and Bulk Water

$n$	$\Delta E(D)/\text{kJ mol}^{-1}$	$\Delta E(\tau_0)/\text{kJ mol}^{-1}$	$\Delta E(\tau_{\text{rot}})/\text{kJ mol}^{-1}$
1.3	$6.9 \pm 0.7$	$17.0 \pm 1.3$	$8.0 \pm 0.8$
2.1	$8.7 \pm 0.6$	$17.8 \pm 1.1$	$8.2 \pm 0.5$
3.7	$10.0 \pm 0.5$	$18.6 \pm 1.0$	$9.7 \pm 1.0$
bulk water	$17.9 \pm 0.9$	$25.9 \pm 1.8$	$13.5 \pm 0.8$

are smaller than those of bulk water and tend to approach them with increasing hydration number. Furthermore, the  $\tau_0$  and  $\langle l \rangle$  of  $\text{H}_2\text{dtoaCu} \cdot n\text{H}_2\text{O}$  are longer than those of bulk water, whereas the  $\tau_{\text{rot}}$  is almost the same as that of bulk water.

The above results indicate that the water molecules responsible for the fast mode are more sparsely packed in the pore than those in bulk water and, therefore, needs to take longer  $\tau_0$  and move longer  $\langle l \rangle$  to find a counter water molecule to reconstruct a hydrogen bond. Instead, once finding the counter water molecule, the reconstruction of the hydrogen bond occurs easily because of smaller hydrogen bonding energy, roughly corresponding to  $\Delta E$ , compared with that in bulk water.

When considering the sparsely packed state described above, it is somewhat strange that the diffusion coefficient  $D$  of the pore water is similar to that of bulk water. This is explained based on eq 7, which is rewritten to  $D = \langle l \rangle^2 / 6\tau_0$ . Both  $\langle l \rangle$  and  $\tau_0$  of the pore water are larger than those of bulk water and they are

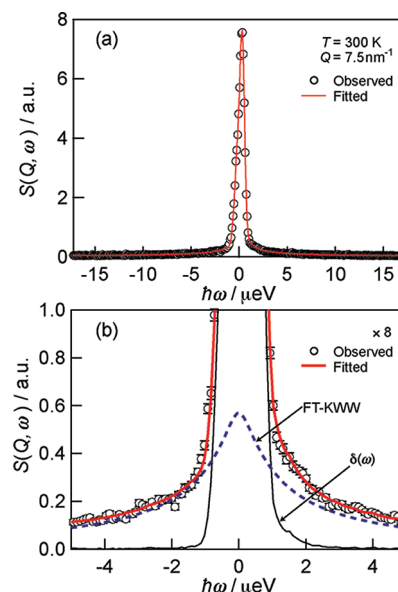


**Figure 7.** QENS profile of  $\text{H}_2\text{dtoaCu} \cdot 3.7\text{H}_2\text{O}$  at  $Q = 7.5 \text{ nm}^{-1}$  and  $T = 300 \text{ K}$  obtained by HFBS (white circles). Solid curve is the result of the fitting to eq 9. The scales of vertical and horizontal axes of panel b are enlarged by 8 and 3.4 times those of panel a, respectively. The thin solid and dashed curves are  $\delta(\omega)$  and FT-KWW in eq 9, respectively.

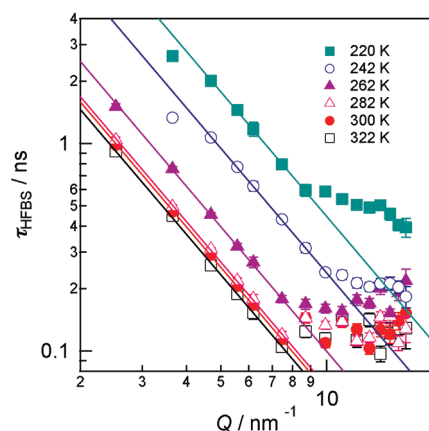


**Figure 8.** Relaxation times of  $\text{H}_2\text{dtoaCu} \cdot 3.7\text{H}_2\text{O}$  as a function of scattering vector  $Q$ . Solid lines are the results of fitting to eq 10.

balanced out. Since  $\Delta E$  of the pore water is different from that of bulk water, the  $D$ 's of the pore and bulk water intersect at ca. 290 K.

**3.4. Quasi-Elastic Scattering Observed by HFBS.** In the measurements of HFBS, quasi-elastic scattering was observed above 220 K. The typical spectrum is shown in Figure 7. The data were fitted to the following equation using DAVE software:

$$S(Q, \omega) = \left[ \text{FT} \left\{ f_1 + f_2 \exp \left( - \left( \frac{t}{\tau_{\text{HFBS}}} \right)^{0.5} \right) \right\} \right] \otimes R(Q, \omega) + \text{BG} \quad (9)$$

where the quasi-elastic scattering is expressed by a stretched exponential function as in the fitting of the slow mode in NSE. FT

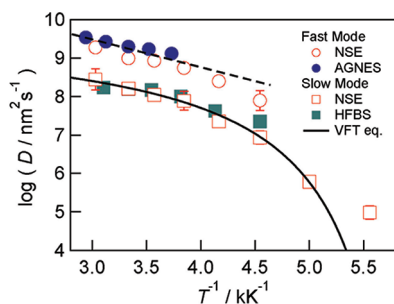


**Figure 9.** Arrhenius plots for diffusion coefficients of  $\text{H}_2\text{dtoaCu}\cdot 3.7\text{H}_2\text{O}$  obtained by AGNES, HFBS, and NSE.

denotes the Fourier transform. The nonexponential parameter  $\beta_{\text{slow}}$  was fixed to 0.5 because the  $\beta_{\text{slow}}$  obtained by NSE was about 0.5 independent of  $Q$ . Scattering from the fast-mode observed by AGNES is regarded to be a flat background in the energy window of HFBS. As shown in Figure 7, the data were well fitted in the whole  $Q$  range. The obtained relaxation times are plotted as a function of  $Q$  in Figure 8. As the power index was almost 2 in the region  $Q < \sim 9\text{ nm}^{-1}$ , diffusion coefficients were obtained from the simple diffusion model

$$\tau = D^{-1}Q^{-2} \quad (10)$$

The present data on HFBS guarantee that at  $Q = 7\text{ nm}^{-1}$ , where the NSE data were taken, the dynamics is in the simple diffusion region. The analysis with the jump-diffusion model, which is performed for the AGNES data, was difficult because the  $Q$  range of HFBS is limited to  $Q < 15\text{ nm}^{-1}$ . The  $Q$  value ( $9\text{ nm}^{-1}$ ) at the crossover between the simple diffusion and the jump diffusion seems to be related to the pore size (ca.  $0.7\text{ nm}$ ); that is,  $2\pi/(0.7\text{ nm}) = 9\text{ nm}^{-1}$ .

The fractions  $f_1 (= f_{\text{nondecay}})$  and  $f_2 (= f_{\text{slow}})$  are plotted in Figure 3; the fast component that cannot be observed by HFBS is assumed to be the same as determined by NSE. The fractions obtained by HFBS agree with those by NSE;  $f_{\text{nondecay}}$  is close to  $f_{\text{slow}}$  at higher temperatures but becomes larger than  $f_{\text{slow}}$  as decreasing temperature.

**3.5. Summary on Dynamics of Water in Copper Rubenate.** All diffusion coefficients obtained from the three spectrometers (AGNES, HFBS and NSE) were shown in Figure 9. Here the diffusion coefficients by NSE were calculated from the relaxation times data and eq 10. Figure 9 clearly shows that two kinds of motion, i.e., the fast mode and slow mode, exist for the water molecules in the pore of  $\text{H}_2\text{dtoaCu}\cdot n\text{H}_2\text{O}$ . The fast mode and slow mode are of Arrhenius type and non-Arrhenius type, respectively. The diffusion coefficients of the slow mode obtained by HFBS and NSE was fitted to the VFT equation

$$D = D_0 \exp\left(-\frac{FT}{(T - T_0)}\right) \quad (11)$$

The parameters  $D_0$ ,  $T_0$ , and  $F$  obtained by the fitting are  $1.4 \pm 0.5 \times 10^9\text{ nm}^2\text{ s}^{-1}$ ,  $163 \pm 6\text{ K}$ , and  $1.7 \pm 0.4$ , respectively. The diffusion coefficients deviate from the VFT equation around 200 K as has been observed in the supercooled water in MCM-41<sup>8,9</sup> and carbon nanotube.<sup>10</sup> However, the neutron scattering experiments with much higher energy resolution are still needed to determine whether the deviation is really due to the “Strong-Fragile” transition of supercooled water reported before or due to the others. Furthermore we should comment on the possibility

that the “Strong-Fragile” transition is not an intrinsic phenomena of bulk water but characteristic of the confined water affected by the pore surface since the previous reports<sup>9–11</sup> did not distinguish the free water and condensed water.

**3.6. Mechanism of Proton Conduction in Copper Rubenate Hydrates.** The proton conductivity mechanism of  $\text{H}_2\text{dtoaCu}\cdot n\text{H}_2\text{O}$  should consist of the proton transfer between the pore wall (NH group of rubeanic acid) and the water molecules and the proton diffusion assisted by the water molecules. Hence, the number of mobile protons, that is the acidity of  $\text{H}_2\text{dtoaCu}$  multiplied by the number of water molecules, and mobility of the water molecules are both important factors for the proton conductivity.

The mechanisms of the proton diffusion assisted by water molecules are roughly divided into two: one is the Vehicle mechanism in which a water molecule having a proton, that is a hydronium ion ( $\text{H}_3\text{O}^+$ ), carries a proton for a long distance and the other is the Grotthuss mechanism in which a hydronium ion reorients and passes a proton to a neighboring water molecules through a hydrogen bond. In the porous systems, it depends on the size and geometry of the pores which mechanism is adopted.

As shown in Figure 6a, the diffusion coefficients of the water molecules in  $\text{H}_2\text{dtoaCu}\cdot n\text{H}_2\text{O}$  do not depend on the hydration number. Taking into consideration that the proton conductivity increases with increasing hydration number, the present result means that the determinant parameter for the proton conductivity is not the diffusivity of the water molecules but the number of mobile protons dissolved in the adsorbed water in the pores. This is consistent with the fact that the activation energy obtained from the temperature dependence of proton conductivity is  $45\text{ kJ mol}^{-1}$ , which is much larger than the activation energy of the water molecules.<sup>14</sup> Once protons are provided to water molecules from the rubeanic acid in the pore wall, the protons are carried by the water molecules through the Grotthuss or Vehicle mechanisms.

It is noteworthy that the jump distance is longer than that of bulk water and the rotational relaxation time is similar to that of bulk water. From these results, we propose that the proton conduction of  $\text{H}_2\text{dtoaCu}\cdot n\text{H}_2\text{O}$  is governed by the intermediate process between the Grotthuss and Vehicle mechanisms: (1) A water molecule catches a proton from the rubeanic acid in the pore wall, (2) next the water molecule travels to a neighboring water molecule and passes the proton through the Grotthuss mechanism, and (3) then the water molecules move to the pore wall and pass the protons to the wall. The rate-determining step of the above process is the proton transfer between the water molecules and rubeanic acid in the pore wall as described before. Unfortunately, this step could not be observed in the present study since it is too slow ( $\tau > 100\text{ ns}$ ).

## 4. CONCLUSION

In this paper, the mechanisms of the first order transition and proton conductivity in copper rubenate hydrates are investigated by QENS techniques from microscopic and dynamical points of view. The adsorbed water is divided into free water having diffusion coefficients similar to those of bulk water at room temperature and condensed water which is about 10 times slower than that of bulk water owing to the interaction with the pore wall. The hydrogen atoms in the pore wall show no relaxation and are observed as a nondecay component. From the NSE measurements, it is found that the first order transition

observed in the heat capacity measurements is a sort of liquid–liquid transition at which the free water is condensed on the pore surface on cooling. This result is consistent with previous results of the neutron diffraction. On cooling the sample, the relaxation time of the condensed water starts to deviate from the VFT equation around 200 K as shown for the water confined in MCM-41 or carbon nanotube. The free water is considered to play an important role for the high proton conductivity of the copper rubeanate hydrate. It is found that a key parameter to control the proton conductivity is the number of protons provided from the pore wall, and the rate of proton transfer between the water molecules and the pore wall is slower than the time scale of the present experiment. To make further investigation on the proton conduction mechanism, the neutron spin echo experiments with Fourier time longer than 100 ns are required.

## AUTHOR INFORMATION

### Corresponding Author

\*E-mail: yamamuro@issp.u-tokyo.ac.jp.

## ACKNOWLEDGMENT

This work is financially supported by Core Research of Evolutional Science & Technology program (CREST) from Japan Science and Technology Agency (JST). This work utilized facilities supported in part by the National Science Foundation under Agreement No. DMR-0944772.

## REFERENCES

- (1) Speedy, R. J.; Angell, C. A. *J. Chem. Phys.* **1976**, *65*, 851–858.
- (2) Sastry, S.; Debenedetti, P. G.; Sciortino, F.; Stanley, H. E. *Phys. Rev. E* **1996**, *53*, 6144–6154.
- (3) Mishima, O.; Stanley, H. E. *Nature* **1998**, *396*, 329–335.
- (4) Debenedetti, P. G. *J. Phys. Condensed Matter* **2003**, *15*, R1669–R1726.
- (5) Angell, C. A. *Annu. Rev. Phys. Chem.* **2004**, *55*, 559–83.
- (6) Teixeira, J.; Bellissent-Funel, M.-C.; Chen, S. H.; Dianoux, A. J. *Phys. Rev. A* **1985**, *31*, 1913–1917.
- (7) Swenson, J.; Bergman, R.; Longeville, S. *J. Chem. Phys.* **2001**, *115*, 11229–11305.
- (8) Liu, L.; Shen, S.-H.; Faraone, A.; Yen, C.-W.; Mou, C.-Y. *Phys. Rev. Lett.* **2005**, *95*, 117802–117805.
- (9) Yoshida, K.; Yamaguchi, T.; Kittaka, S.; Bellissent-Funel, M.-C.; Fouquet, P. *J. Chem. Phys.* **2008**, *129*, 054702–054712.
- (10) Chu, X.-Q.; Kolesnikov, A. I.; Moravsky, A. P.; Garcia-Sakai, V.; Chen, S.-H. *Phys. Rev. E* **2007**, *76*, 021505–021510.
- (11) Mamontov, E. *J. Chem. Phys.* **2005**, *123*, 171101–171104.
- (12) Kamitakahara, A. W.; Wada, N. *Phys. Rev. E* **2008**, *77*, 041503–041512.
- (13) Malikova, N.; Cadène, A.; Dubois, E.; Marry, V.; Durand-Vidal, S.; Turq, P.; Breu, J.; Longeville, S.; Zanotti, J.-M. *J. Phys. Chem. C* **2007**, *111*, 17603–17611.
- (14) Kitagawa, H.; Nagao, Y.; Fujishima, M.; Ikeda, R.; Kanda, S. *Inorg. Chem. Commun.* **2003**, *6*, 346–348.
- (15) Yamada, T.; Yonamine, R.; Yamada, T.; Kitagawa, H.; Yamamuro, O. *J. Phys. Chem. B* **2010**, *114*, 8405–8409.
- (16) Yamamuro, O.; Inamura, Y. *Hamon* **2007**, *17*, 85–89.
- (17) Meyer, A.; Dimeo, R. M.; Gehring, P. M.; Neumann, D. A. *Rev. Sci. Instrum.* **2003**, *74*, 2759.
- (18) Azuah, R. T.; Kneller, L. R.; Qiu, Y.; Tregenna-Piggott, P. L. W.; Brown, C. M.; Copley, J. R. D.; Dimeo, R. M. *J. Res. Natl. Inst. Stand. Technol.* **2009**, *114*, 341–358.
- (19) Rosov, N.; Rathgeber, S.; Monkenbusch, M. *ACS Symp. Ser.* **2000**, *739*, 103–116.

(20) Zhang, Q. M.; Feng, Y. P.; Kim, H. K.; Chan, M. H. W. *Phys. Rev. Lett.* **1986**, *57*, 1456–1459.

(21) Migone, A. D.; Li, Z. R.; Chan, M. H. W. *Phys. Rev. Lett.* **1984**, *53*, 810–813.

(22) Brovchenko, I.; Oleinikova, A. *J. Phys. Chem. C* **2007**, *111*, 15716–15725.